Heteronuclear NMR and Crystallographic Studies of Wild-Type and H187Q *Escherichia coli* Uracil DNA Glycosylase: Electrophilic Catalysis of Uracil Expulsion by a Neutral Histidine 187†

Alexander C. Drohat,‡ Gaoyi Xiao,‡ Maria Tordova,‡ Jaya Jagadeesh,‡ Krzysztof W. Pankiewicz,§ Kyoichi A. Watanabe,§ Gary L. Gilliland,‡ and James T. Stivers*,‡

Center for Advanced Research in Biotechnology of the University of Maryland Biotechnology Institute and the National Institute for Standards and Technology, 9600 Gudelsky Drive, Rockville, Maryland 20850, and Pharmasset, Inc., 1925 Century Boulevard, Suite 4, Atlanta, Georgia 30345

Received May 12, 1999; Revised Manuscript Received June 30, 1999

ABSTRACT: The nature of the putative general acid His187 in the reaction catalyzed by *Escherichia coli* uracil DNA glycosylase (UDG) was investigated using X-ray crystallography and NMR spectroscopy. The crystal structures of H187Q UDG, and its complex with uracil, have been solved at 1.40 and 1.60 Å resolution, respectively. The structures are essentially identical to those of the wild-type enzyme, except that the side chain of Gln187 is turned away from the uracil base and cannot interact with uracil O2. This result provides a structural basis for the similar kinetic properties of the H187Q and H187A enzymes. The ionization state of His187 was directly addressed with $^{1}H-^{15}N$ NMR experiments optimized for histidine ring spin systems, which established that His187 is *neutral* in the catalytically active state of the enzyme (pK_a <5.5). These NMR experiments also show that His187 is held in the $N^{\epsilon_2}-H$ tautomeric form, consistent with the crystallographic observation of a 2.9 Å hydrogen bond from the backbone nitrogen of Ser189 to the ring N^{δ_1} of His187. The energetic cost of breaking this hydrogen bond may contribute significantly to the low pK_a of His187. Thus, the traditional view that a *cationic* His187 donates a proton to uracil O2 is incorrect. Rather, we propose a concerted mechanism involving general base catalysis by Asp64 and electrophilic stabilization of the developing enolate on uracil O2 by a *neutral* His187.

The enzymatic repair of damaged bases in DNA often begins with hydrolysis of the *N*-glycosidic bond to release the damaged base. An important question regarding the mechanism of this reaction is whether the enzyme activates the base for departure. It is reasonable to expect that a *purine* base may be activated by protonation or alkylation at N1, N3, or N7, and this is supported by solution and enzymatic studies (*1*, *2*). However, it is highly questionable whether an enzyme can activate a damaged *pyrimidine* base by protonation at O2 or O4, due to the extremely low pK_a (∼−3.4) of these carbonyl oxygens (*3*). The mechanism of pyrimidine-specific glycosylases may therefore proceed without preequilibrium protonation of the leaving group base or by a concerted mechanism in which a proton or a hydrogen bond is donated to stabilize the developing enolate in the transition state.

The DNA repair enzyme uracil DNA glycosylase (UDG), which catalyzes the hydrolysis of the *N*-glycosidic bond of premutagenic uracil bases in DNA, provides an attractive system to study this question in detail. A general acid−base mechanism has been proposed for UDG whereby a cationic histidine residue donates a proton to uracil O2 and an aspartate residue activates a water molecule for nucleophilic attack at C1′ of the deoxyribose (*4*−*6*). Although it has recently been proposed that His187 may be neutral during the catalytic cycle of UDG (*7*, *8*), direct evidence of the ionization state of His187 in the free enzyme and the enzyme−substrate complex is lacking.

In the preceding paper of this issue we provide evidence, from mutagenesis and pH−rate studies of *Escherichia coli* UDG, that supports a role for Asp64 as the general base (*9*). Additionally, we find that conversion of His187 to glutamine or alanine by mutagenesis results in as much as a 4.8 kcal/mol destabilization of the transition state (*9*). However, the pH dependence of the kinetic parameters provides no evidence for a catalytically essential acidic group over the pH range 5−10 in the free enzyme or the enzyme−substrate complex (*9*). Taken together, the structural, mutagenesis, and kinetic evidence indicates that His187 forms an essential interaction with uracil O2 in the transition state. However, the important question of whether His187 is cationic with an exceptionally high pK_a (>10) or neutral with an unusually low pK_a (<5) remains unanswered.

Bachovchin, among others, has shown that ^{15}N NMR spectroscopy is an excellent method to unambiguously determine the ionization state of a histidine ring in a protein or enzyme (*10*−*13*). This is because the ^{15}N chemical shift of an imidazole nitrogen depends dramatically on its electronic hybridization state and whether it has a bonded hydrogen atom (*14*, *15*). Thus, the two ^{15}N resonances from

† This work was supported by NIH Grant GM56834 (to J.T.S.) and the National Institute for Standards and Technology. A.C.D. is a National Research Council Postdoctoral Research Associate.

* Address correspondence to this author: phone, 301-738-6264; fax, 301-738-6255; e-mail, stivers@carb.nist.gov.

‡ Center for Advanced Research in Biotechnology.

§ Pharmasset, Inc.

10.1021/bi9910880 CCC: $18.00
Published on Web 08/24/1999

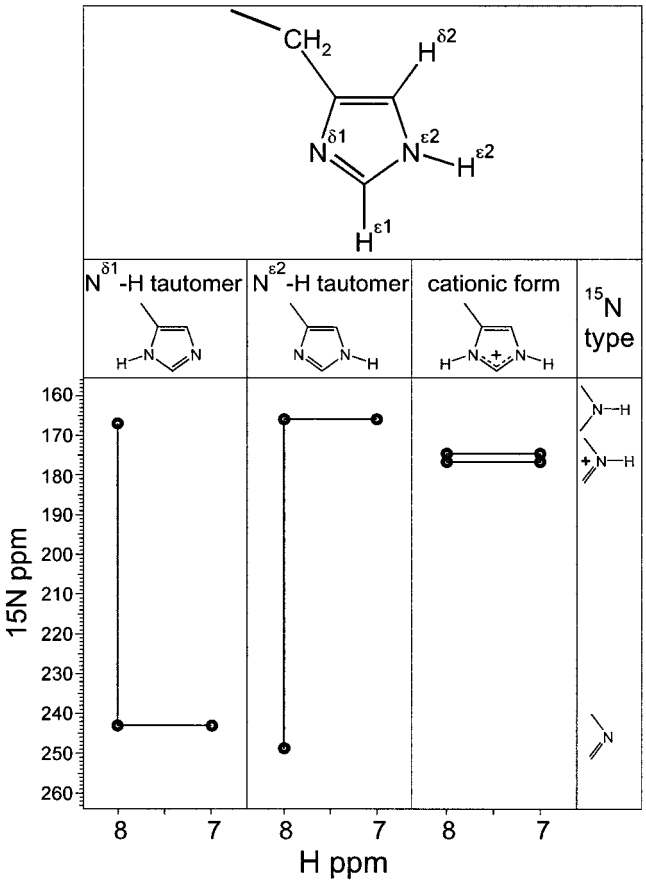

FIGURE 1: Nomenclature used for histidine rings and peak patterns expected in the 2D $^1H-^{15}N$ LR-HSQC spectra for the three possible tautomeric states of a histidine ring (*13*). The ^{15}N chemical shifts are from studies of histidine, N^{δ_1}-methylhistidine, and N^{ϵ_2}-methylhistidine in water at 25 °C (*16*), and the ^1H chemical shifts are from histidine residues in random coils (*37*). The ^{15}N chemical shifts are referenced to external liquid ammonia and were converted by subtracting the reported value, referenced to 1 M HNO_3, from 377.5 ppm (*13*). The ring nitrogens have three two-bond J couplings to the carbon-attached protons ($N^{\delta_1}-H^{\epsilon_1}$, $N^{\epsilon_2}-H^{\epsilon_1}$, and $N^{\epsilon_2}-H^{\delta_2}$), which are usually observed in the 2D LR-HSQC, and one three-bond *J* coupling ($N^{\delta_1}-H^{\delta_2}$), which is usually not observed (*13*, *15*, *17*).

a neutral histidine ring will differ by about 80 ppm, whereas the ^{15}N resonances from a cationic histidine ring will differ by only ~2 ppm (Figure 1) (*11*, *15*, *16*). The sensitivity and resolution of the ^{15}N spectrum can be significantly improved by using a two-dimensional $^1H-^{15}N$ long-range HSQC (LR-HSQC) experiment, which correlates the two histidine ring nitrogens with the two carbon-attached protons as shown in Figure 1 (*13*, *17*).

We have investigated the nature of uracil leaving group activation by His187 in *E. coli* UDG using crystallographic and heteronuclear NMR methods. Despite the large size of the enzyme (25.5 kDa) and the presence of 13 other histidine residues, we were able to unambiguously assign the NMR resonances of His187 using the approaches of mutagenesis and selective labeling with $^{13}C-^{15}N$-enriched amino acids. Using 2D LR-HSQC experiments, we have found that His187 is neutral in the free enzyme over the pH range of 5.5−9.5 and in the UDG complex with a stable 2′-fluoro-2′-deoxyuridine substrate analogue (*18*) at pH 6.0 and 6.8. Thus, the pK_a of His187 is below 5.0 in the free enzyme and below 5.5 in the enzyme−substrate complex. In contrast to the proposal that a cationic His187 donates a proton to uracil O2 (*4*−*6*), our results indicate that His187 facilitates departure of the uracil leaving group by donating a neutral hydrogen bond to uracil O2 in the transition state. The high-resolution X-ray crystal structures of H187Q UDG and the H187Q−uracil product complex show that the overall conformation and orientation of the active site residues of H187Q UDG are very similar to those of wild-type UDG. Surprisingly, the side chain of Gln187 exhibits no direct interaction with the bound uracil base. This provides a structural explanation for the similar kinetics and DNA binding properties of the H187Q and H187A enzymes (*9*).

EXPERIMENTAL PROCEDURES[1]

General. Wild-type and H187Q UDG from *E. coli* strain B were produced using a T7 polymerase-based expression system and purified to >99% homogeneity as described (*7*). The stable substrate analogue pU$^{\beta}$**P**A,[2] which contains deoxyuridine with a 2′-β-fluorine substitution (U$^{\beta}$) and the fluorescent reporter 2-aminopurine (**P**), was synthesized and purified as previously described (*9*, *18*). MALDI-TOF mass spectrometry analysis of pU$^{\beta}$**P**A gave a mass of 953.7, compared to the calculated mass of 952.6 (Midland Certified Reagent Co., Midland, TX).

Isotopic Labeling of UDG for Heteronuclear NMR. Uniformly ^{15}N-labeled UDG samples were prepared by growing the BLR(DE3)plysS cells, containing the pET21-(UDG) or pET21(H187Q) plasmid, in MOPS minimal media (*19*) with 1.0 g/L ^{15}N-labeled (>99 atom %) ammonium chloride (Martek Biosciences, Columbia, MD) as the sole nitrogen source. The UDG sample containing $^{13}C-^{15}N$-labeled histidine and proline residues was prepared by growing the UDG expression cells in MOPS minimal media containing 0.2 g/L each of the natural L-amino acids except histidine and proline. When the OD^{600} reached ~0.8, the uniformly $^{13}C-^{15}N$-labeled L-histidine (Martek Biosciences) and uniformly $^{13}C-^{15}N$-labeled L-proline (Cambridge Isotope Laboratories, Andover, MA) were added at a final concentration of 0.1 g/L. The cells were induced 15 min after the labeled amino acids were added.

Crystallization and X-ray Data Collection. The H187Q *E. coli* UDG was crystallized in the same space group and under the same conditions as described for wild-type *E. coli* UDG (*7*). The H187Q−uracil complex crystals were prepared by soaking the H187Q crystals in stabilizing buffer

[1] Certain commercial equipment, instruments, and materials are identified in this paper in order to specify the experimental procedure. Such identification does not imply recommendation or endorsement by the National Institute of Standards and Technology, nor does it imply that the material or equipment identified is necessarily the best available for the purpose.

[2] Abbreviations: 2′-β-F, 2′-β-fluorine isomer of deoxyuridine; 2′-β-H, 2′-β-hydrogen; pU$^{\beta}$**P**A, stable trinucleotide substrate analogue containing 2′-β-F-deoxyuridine 5′-phosphate (pU$^{\beta}$), 2-aminopurine deoxyribonucleoside (**P**), and adenosine deoxynucleotide (A); DSS, 2,2-dimethyl-2-silapentane-5-sulfonic acid; HSQC, $^1H-^{15}N$ heteronuclear single-quantum coherence; IMCA-CAT, Industrial Macromolecular Crystallography Association Collaborative Access Team; LR-HSQC, long-range $^1H-^{15}N$ heteronuclear single-quantum coherence; CBCA-(CO)NH, correlation experiment which correlates the $^{13}C^{\alpha}$ and $^{13}C^{\beta}$ resonances of residue *i* with the NH of residue *i* + 1; MALDI-TOF, matrix-assisted laser desorption ionization time of flight; NOE, nuclear Overhauser effect; NOESY, nuclear Overhauser effect spectroscopy; TPPI, time-proportional phase incrementation; **P**, 2-aminopurine.

Table 1: X-ray Data and Refinement Statistics for H187Q and Its Uracil Complex

parameter	H187Q UDG	H187Q−uracil
data statistics		
X-ray source	Synchrotron source at APS	Bruker rotating anode
wavelength (Å)	0.95	1.54
space group	$P2_12_12_1$	$P2_12_12_1$
unit cell (Å)	$a = 54.1$, $b = 59.0$, $c = 63.8$	$a = 54.4$, $b = 59.4$, $c = 64.2$
resolution with $I \geq 1.5\sigma$ (Å)	1.40	1.60
unique reflections	77493	28096
completeness (%)	100.0	92.4
redundancy	4.4	4.9
R_{merge} (%)[a]	10.5	7.6
refinement statistics		
crystallographic *R*-factor[b]	0.179	0.178
no. of residues	225	225
no. of waters	298	248
RMSDs from ideal		
bond distances (Å)	0.010	0.006
angle distances (Å)	0.028	0.022
planarity (Å)	0.028	0.024

[a] $R_{merge} = \sum|I_{obs} - I_{av}|/\sum I_{obs}$, where the summation is over all reflections. [b] *R*-factor $= \sum|F_o - F_c|/\sum|F_c|$, where F_o and F_c are the observed and calculated structure factors.

containing 6.0 mM uracil for 3 h. The diffraction data for free H187Q UDG were collected at the IMCA-CAT beamline 17-ID of the Advanced Photon Source (Argonne, IL). The diffraction data for the H187Q−uracil complex were collected with a HISTAR electronic area detector on a rotating anode X-ray generator (Brüker AXS, Madison, WI). During data collection on both instruments, Oxford Cryostreams (Oxford Cryostreams, U.K.) maintained the crystals near 115 K. The diffraction data were indexed and processed with X-GEN (Molecular Simulations, Inc., San Diego, CA) (*20*). The diffraction results are summarized in Table 1.

Crystal Structure Refinement. The starting model for the refinements of free H187Q UDG and the H187Q−uracil complex structures was the 1.43 Å resolution structure of the Y19H *E. coli* UDG glycerol complex (*7*). The residues His187 and His19 were changed to alanine in the starting models to avoid biasing the refinement. The two glycerol molecules were omitted, and the first 200 water molecules were retained in the model. This model was refined with SHELX-97 (*21*, *22*) against data for H187Q UDG and its complex with uracil. After 10 cycles of refinement, the residues Gln187 and Tyr19 were clearly defined in the $F_o - F_c$ maps of both structures, and the uracil was clearly defined in the $F_o - F_c$ map of the H187Q−uracil complex. The molecular display and map fitting program TURBO-FRODO (*23*) was used to examine and adjust the structure during the refinement process. The program PROCHECK (*24*) was used to examine the stereochemical parameters of the final structures. The refinement results are summarized in Table 1.

NMR Spectroscopy. NMR experiments were conducted on Bruker DRX500 and DRX600 spectrometers, each equipped with four frequency channels and a triple-axis gradient $^1H-^{13}C-^{15}N$ probe. Proton chemical shifts are reported with respect to external DSS. The ^{13}C and ^{15}N chemical shifts were indirectly referenced to DSS and liquid NH_3, respectively, using the zero point frequency ratios $^{13}C/^1H = 0.251449530$ and $^{15}N/^1H = 0.101329118$ (*25*). Experiments were conducted with 1 s recycle delays, and quadrature detection in the indirect dimensions was obtained by States−TPPI phase cycling (*26*). Data were processed on a Silicon Graphics workstation using the NMRPipe computer program (*27*). Data in the ^{15}N dimension were extended 2-fold using the standard linear prediction routine in NMRPipe. In general, the NMR samples contained 0.3−1.0 mM UDG, 0.01 M NaH_2PO_4, pH 6.6 (unless noted otherwise), 0.25 M NaCl, and 5% D_2O.

The conventional 2D $^1H-^{15}N$ HSQC experiments (*28*), for observation of backbone amide $^1H-^{15}N$ correlations, were in general collected at 25 °C with 16−24 scans, 64 complex t_1 points and 1024 complex t_2 points, and with ^{15}N decoupling by WALTZ-16 (*29*) with a 1.0 kHz field. For the 0.6 mM $^{13}C-^{15}N$ His-Pro-labeled wild-type UDG sample, the 2D $^1H-^{15}N$ HSQC was collected at 600 MHz with acquisition times of 29.2 ms in t_1 and 122 ms in t_2 and with the ^1H and ^{15}N carriers at 4.78 and 118.4 ppm. For the 0.5 mM uniformly ^{15}N-labeled H187Q UDG sample, the 2D $^1H-^{15}N$ HSQC was collected at 500 MHz with acquisition times of 35.1 ms in t_1 and 114 ms in t_2 and with the ^1H and ^{15}N carriers at 4.81 and 118.4 ppm.

The 2D $^1H-^{15}N$ LR-HSQC experiments were collected to correlate the histidine ring N^{δ_1} and N^{ϵ_2} nitrogens with the H^{δ_2} and H^{ϵ_1} ring protons (Figure 1). This experiment was simply a conventional HSQC used for backbone amide correlations (*28*) collected with a dephasing delay of 22 ms in order to observe signals from the weak two-bond $^2J_{NH}$ couplings in the histidine rings and suppress signals from the one-bond J_{NH} amide couplings (*13*). The LR-HSQC spectra for the uniformly ^{15}N-labeled wild-type UDG (0.8 mM) and H187Q UDG (0.4 mM) samples were collected at 500 MHz at 25 or 30 °C and with the ^1H and ^{15}N carriers at 4.81 and 210.4 ppm, respectively. The spectra were collected at pH values of 5.5, 6.6, 7.5, 8.5, and 9.5 for the wild-type sample and at pH values of 6.6 and 7.5 for the H187Q sample. The ^{15}N dimension was collected with 23−40 complex points and a 110 ppm sweep width, and the ^1H dimension was collected with 1024 complex points and a 12.0 ppm sweep width. The complexes of uniformly ^{15}N-labeled wild-type and H187Q UDG with pU$^{\beta}$**P**A were collected at 600 MHz at 25 °C, with the ^1H and ^{15}N carriers at 4.79 and 210.4 ppm, respectively. The wild-type and H187Q UDG samples at pH 6.8 contained 0.5 mM UDG and 1.0 mM pU$^{\beta}$**P**A, and the wild-type sample at pH 6.0 contained 0.25 mM UDG and 0.5 mM pU$^{\beta}$**P**A. The ^{15}N dimension was collected with 32 complex points and a 120 ppm sweep width, and the ^1H dimension was collected with 1024 complex points and a 16.0 ppm sweep width. Decoupling of ^{15}N was accomplished with the GARP sequence (*30*) using a 1.39 kHz field.

The 3D ^{15}N-edited NOESY experiment (*31*) was collected on a 1.0 mM uniformly ^{15}N-labeled wild-type UDG sample, pH 7.50, at 500 MHz and 25 °C. The ^1H and ^{15}N carriers were at 4.76 and 120.4 ppm, respectively, and 16 scans were collected per FID. The acquisition times and number of complex points were 11.2 ms and 90 points in t_1 (^1H), 14.8 ms and 30 points in t_2 (^{15}N), and 114 ms and 1024 points in t_3 (^1H). Decoupling of ^{15}N was accomplished with WALTZ-16 (*29*) at a 1.39 kHz field.

The CBCA(CO)NH experiment (*32*) was collected on a 0.6 mM uniformly $^{13}C-^{15}N$ His-Pro-labeled wild-type UDG sample. The experiment was executed in a 1D mode by

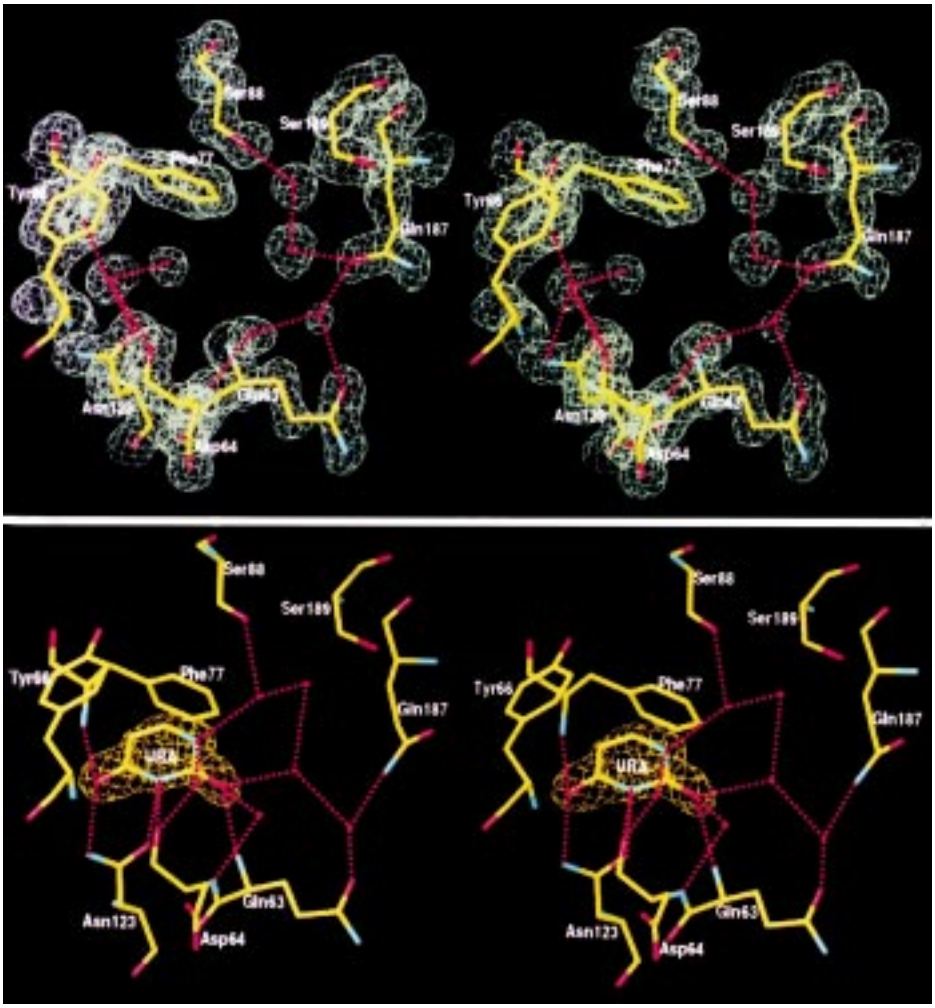

FIGURE 2: Electron density maps at the active site of H187Q UDG. (A, top) $2F_o - F_c$ electron density map, contoured at 1.5σ, showing the active site residues of free H187Q UDG. (B, bottom) Omit $F_o - F_c$ electron density map, contoured at 4.0σ, for the uracil product in the active site of H187Q UDG. Dashed lines illustrate potential hydrogen bonds (distance < 3.5 Å). This figure and Figure 3 were prepared with TURBO-FRODO (*23*).

setting the ^{13}C and ^{15}N evolution periods to 3 μs and collecting 1024 scans. Thus, a backbone amide ^1H signal was only detected for those histidine residues that were preceded by a histidine or proline residue in the primary sequence of UDG. The ^1H acquisition time was 61 ms, and the ^1H, ^{13}C, and ^{15}N carriers were set to 4.78, 48.4, and 117.4 ppm, respectively. Decoupling of ^{15}N was by WALTZ-16 (*29*) with a 1.0 kHz field.

RESULTS AND DISCUSSION

Crystal Structures of Free H187Q and the H187Q−Uracil Complex. The crystal structures of free H187Q UDG and the H187Q−uracil complex have been determined at 1.40 and 1.60 Å resolution, respectively. The final coordinates of both structures contain 225 of the 229 amino acid residues in *E. coli* UDG, as the four N-terminal residues were not observed. The structures of free H187Q UDG and the H187Q−uracil complex contain 298 and 248 water molecules, respectively. Ramachandran plots (*33*) for both structures show 92.1% of the residues in the most favorable region and no residues in the disallowed regions. A comparison of the $2F_o - F_c$ electron density maps and final coordinates shows good agreement between the two structures. An electron density map of the active site region from each structure is shown in Figure 2. The final coordinates for the structures have been deposited at the Protein Data Bank under the ID codes 4EUG for free H187Q and 5EUG for the H187Q−uracil complex.

Structural Comparisons at the Active Site of H187Q and Wild-Type UDG. The crystal structures of H187Q UDG and its complex with uracil are nearly identical to those of wild-type UDG and its uracil complex when the orientations of active site residues are compared. As shown in Figure 3, the uracil recognition pocket is formed by the conserved residues Gln63, Asp64, Tyr66, Phe77, Ser88, Asn123, His187, and Ser189. When the C^α atoms of these residues in H187Q and wild-type structures are superimposed, the RMSD is ≤0.23 Å for all active site residues and ≤0.44 Å for the His187−Gln187 pair. The orientation of the uracil molecule in each structure is also essentially the same. Thus, the H187Q mutation results in only minor and local perturbations to the structure of the free enzyme and its complex with uracil.

Although the side chain amide group of Gln187 was expected to form a hydrogen bond with uracil O2 in a manner similar to that of His187, the structure reveals that the side chain of Gln187 is directed away from the uracil base (Figure 3). The χ_1 rotamer adopted by Gln187 in the H187Q−uracil

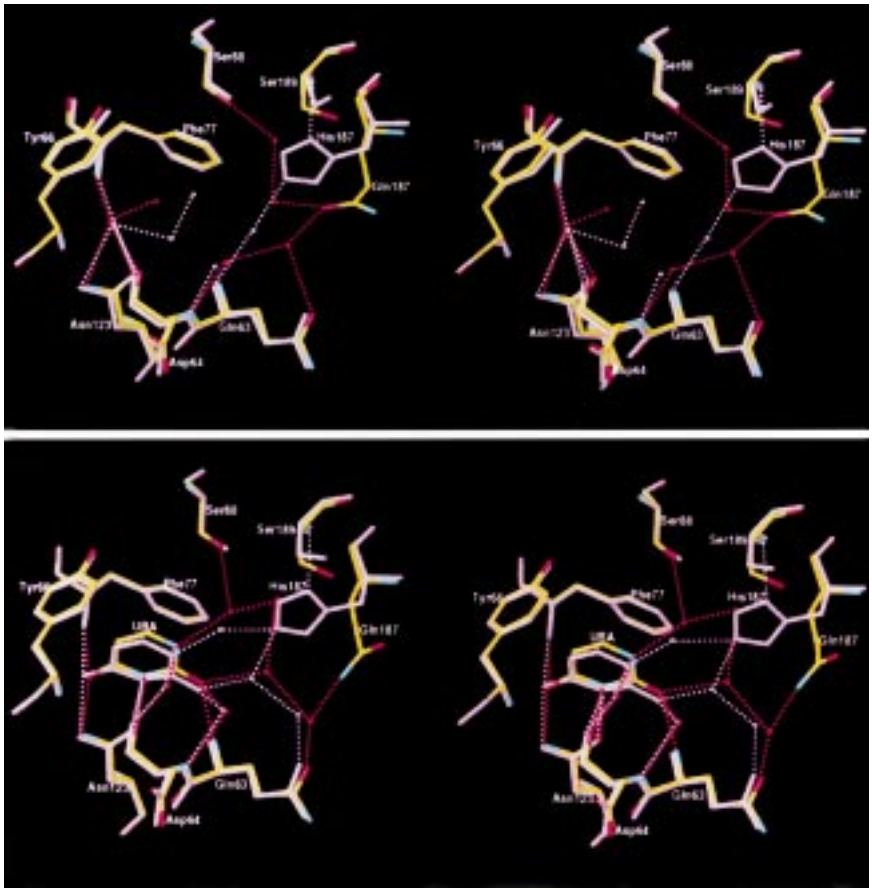

FIGURE 3: Alignment of the active site residues of H187Q and wild-type UDG. (A, top) The active site residues of free H187Q (colored by atom type) align well with those of wild-type UDG (in pink), with an RMSD for C^{α} superposition of 0.23 Å. (B, bottom) Active site residues in the H187Q−uracil complex also align well with the UDG−uracil complex, giving an RMSD for C^{α} superposition of 0.14 Å. Dashed lines illustrate potential hydrogen bonds (distance < 3.5 Å).

complex is very close to a preferred glutamine χ_1 rotamer and differs by 97° from the χ_1 rotamer of His187 (*7*). This orientation results in a longer distance of 6.6 Å from Gln187 N^{ϵ_2} to uracil O2, compared to 4.2 Å from His187 N^{ϵ_2} to uracil O2. Thus, Gln187 appears to have no interaction with uracil, whereas H187 interacts with uracil O2 indirectly through a water-mediated hydrogen bond in the *E. coli* UDG−uracil complex and a direct hydrogen bond in the complex of human UDG with uracil and abasic DNA (*7*, *34*). This is in agreement with the observation that the H187Q and H187A mutations have nearly identical damaging effects (*9*). In other words, Gln187 shows no greater interaction with uracil during catalysis than does Ala187.

General NMR Assignment Strategy for His187. In the absence of complete chemical shift assignments for the backbone and side chain resonances, the selective assignment of histidine ring ^{1}H and ^{15}N resonances (Figure 1) in a protein or enzyme can be accomplished using three general approaches. First, *all* histidine residues except the one of interest can be mutated, as was done by Lodi and Knowles for two of the three histidines in triosephosphate isomerase (*12*). Second, a *single* histidine mutant can be generated, and its NMR spectrum can be compared with that of the wild-type enzyme to identify the signal which is missing in the mutant spectrum, as done by Bycroft and Fersht for subtilisin BPN′ (*35*). Third, the side chain resonances of a specific histidine can be assigned by scalar or NOE correlations with its backbone resonances (*13*), which in turn may be assigned using selective ^{13}C−^{15}N labeling approaches. Selective labeling is particularly effective for histidine residues because cross-labeling of the ^{13}C and ^{15}N isotopes from histidine to other amino acids by metabolic scrambling is minimal (*36*). In addition, if the histidine residue of interest is preceded by another residue, such that the X^n−His^{n+1} pair is unique in the primary sequence, then the histidine backbone resonances will show exclusive scalar connectivities to the preceding residue if it is also selectively labeled with ^{13}C and ^{15}N. The first approach (mutation of all histidine residues except His187) was impractical for UDG, since it contains 14 histidine residues. Thus, assignment of the His187 ring ^{1}H and ^{15}N resonances was made by comparisons of the 2D ^{1}H−^{15}N LR-HSQC spectra for H187Q and wild-type UDG and by selective ^{13}C and ^{15}N labeling to assign the His187 backbone resonances. The backbone amide proton was then correlated with the His187 H^{δ_2} ring resonance using ^{15}N-edited NOE spectroscopy.

Ionization State of His187 in Free UDG. The 2D ^{1}H−^{15}N LR-HSQC experiment, when optimized for histidine ring spin systems, correlates the N^{δ_1} and N^{ϵ_2} resonances with the carbon-attached H^{δ_2} and H^{ϵ_1} resonances via scalar couplings (Figure 1) (*13*, *17*). It is clear from the expected peak patterns for a neutral vs cationic histidine ring shown in Figure 1 that the ionization state of a histidine ring can be readily obtained (*13*). In addition, the tautomeric form of a neutral

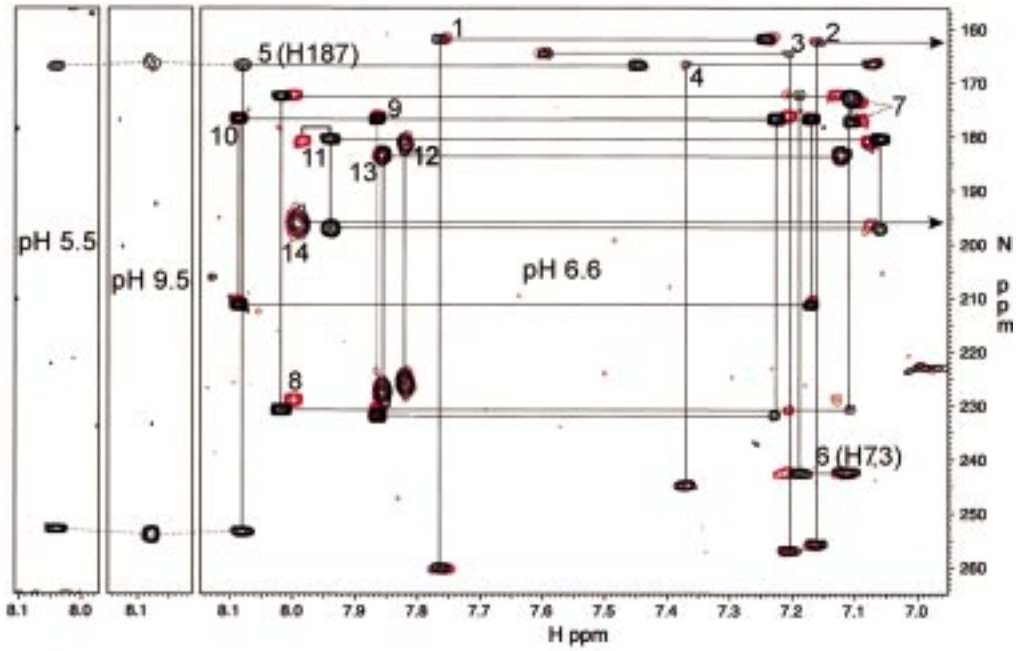

FIGURE 4: 2D $^{1}H-^{15}N$ LR-HSQC spectra of free wild-type UDG (black peaks) and H187Q UDG (red peaks) at pH 6.6 and free wild-type UDG at pH 5.5 and 9.5. The spin systems are connected by solid black lines and numbered randomly with the assignment given for His187 and His73 (see text). Strip plots of the downfield resonances of His187 at pH 5.5 and 9.5 are also shown. As indicated by the arrows, the H^{δ_2} protons of systems 2 and 13 resonate upfield at 6.80 and 6.02 ppm, respectively.

histidine ring can be revealed, providing unambiguous evidence as to which nitrogen is a hydrogen bond donor or acceptor (Figure 1).

The LR-HSQC experiment was conducted with uniformly ^{15}N-labeled samples of wild-type and H187Q UDG at pH 6.6. The LR-HSQC spectrum of free wild-type UDG shows 14 histidine ring spin systems, one for each of the 14 histidines in the UDG primary sequence (Figure 4, black peaks). Examination of Figure 4 shows that, for each of the histidine ring systems identified in the wild-type spectrum, a corresponding system is seen for the H187Q spectrum (red peaks), except for the system labeled 5 (H187). Therefore, system 5 in the wild-type UDG spectrum was assigned to His187.

With the assignment of the His187 ring system established, a comparison of its peak pattern in Figure 4 with the expected patterns for neutral and cationic histidine rings (Figure 1) shows that His187 is *neutral* in the free enzyme at pH 6.6. To set an upper limit for the pK_a of His187, the LR-HSQC spectra of the free enzyme were also acquired at pH 5.5, 7.5, 8.5, and 9.5. The downfield resonances of His187 at the limiting pH values of 5.5 and 9.5 are shown as strip plots in Figure 4. It is clear from these spectra that the nitrogen chemical shifts for His187 remain the same at pH 5.5 and 9.5 as compared to pH 6.6, establishing that His187 is also neutral at these pH values. This result requires that the pK_a of His187 is $\leq$5.0 in the free enzyme. A pK_a $\leq$5.0 is in agreement with the pH dependence of k_{cat}/K_m for UDG, which shows no evidence for an essential protonated group over the pH range 5−10 (*9*). The nitrogen-attached H^{ϵ_2} proton of His187 is not observed in a conventional 2D $^{1}H-^{15}N$ HSQC experiment optimized for one-bond $^{1}H-^{15}N$ correlations, indicating that this proton exchanges freely with solvent. This solution NMR result is consistent with the UDG crystal structure, which shows that His187 $N^{\epsilon_2}-H$ is hydrogen bonded to an ordered water molecule.

Selective Labeling Confirms the Chemical Shift Assignments of His187 in Free UDG. To confirm that the mutagenesis approach provided the correct assignments for the His187 ring correlations, the backbone H^N and ^{15}N resonances of His187 were assigned using selective $^{13}C-^{15}N$ labeling, and these resonances were correlated to the H^{δ_2} ring proton of His187 using a 3D ^{15}N-edited NOESY experiment (*31*). Since His187 is the only histidine residue in the primary sequence that is preceded by a proline residue (Pro186), selective ^{13}C and ^{15}N labeling of both histidine and proline residues was performed. The rationale for this approach is that the CBCA(CO)NH experiment can be used to correlate the $^{13}C^{\alpha}$ and $^{13}C^{\beta}$ resonances of residue *i* with the backbone H^N and ^{15}N resonances of residue $i + 1$ (*32*). Accordingly, the $^{13}C^{\alpha,\beta}$ resonances of Pro186 can be correlated with the backbone H^N and ^{15}N resonances of His187, with the signal observed on the H^N of His187. There is also a His−His pair in the primary sequence of UDG (His180−His181), so we expected to observe an additional H^N resonance from His181 due to the labeling of this sequential pair. Since the selective labeling protocol negated resonance overlap and because the 3D version of the CBCA(CO)NH yielded very little signal due to fast T_2 relaxation effects, a 1D version of this experiment was used. In the 1D version, the detected amide proton signal is edited for the attached ^{15}N as well as scalar connectivities to the $^{13}C^{\alpha}$ and $^{13}C^{\beta}$ resonances of the preceding residue.

As expected, only two H^N resonances are observed in the 1D CBCA(CO)NH spectrum (Figure 5A). To determine which of the two H^N resonances is from His187, we compared the 2D $^{1}H-^{15}N$ HSQC spectra of wild-type UDG (selectively $^{13}C-^{15}N$-labeled at His and Pro residues) and H187Q UDG (uniformly ^{15}N-labeled). Figure 5B shows that for each backbone amide correlation peak seen in the wild-type UDG spectrum (black, *histidines only*), a nearly overlapping peak is seen in the H187Q spectrum (red, all

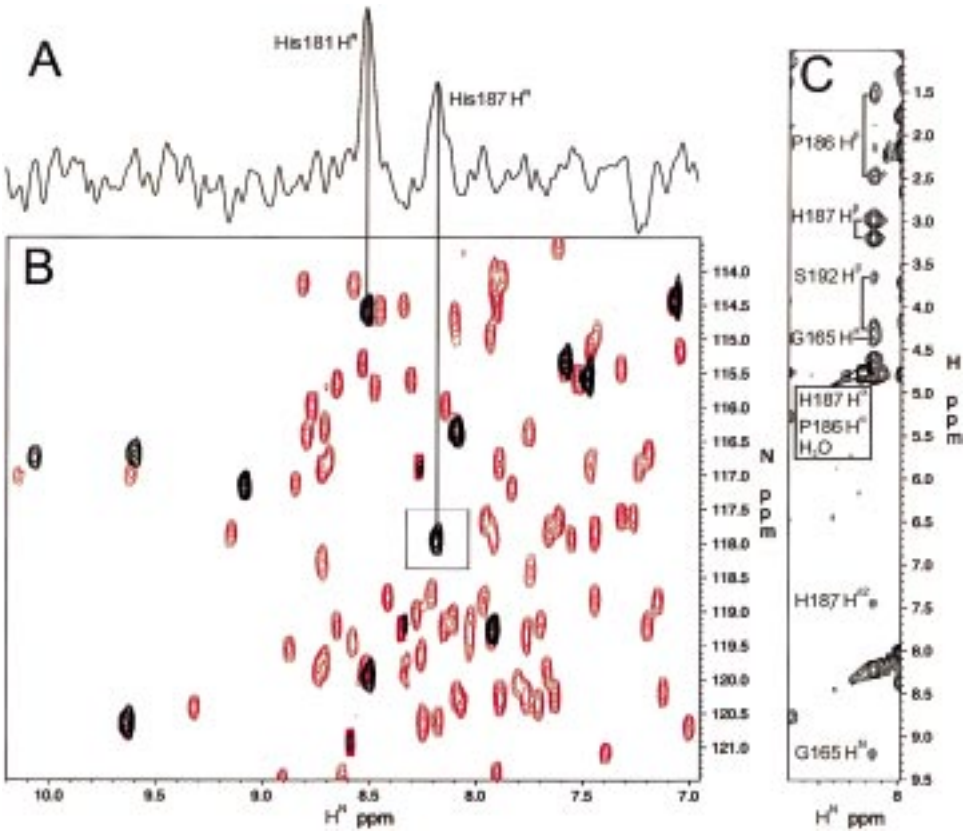

FIGURE 5: Assignment of the His187 backbone $^1H-^{15}N$ and ring H^{δ_2} chemical shifts. (A) The 1D CBCA(CO)NH spectrum of wild-type UDG selectively labeled with $^{13}C-^{15}N$ histidine and proline residues shows the expected two H^N resonances for His181 and His187 (see text). (B) An overlay of the 2D $^1H-^{15}N$ HSQC spectra of wild-type $^{13}C-^{15}N$ His-Pro-labeled UDG (black peaks) and uniformly ^{15}N-labeled H187Q (red peaks) shows that the only wild-type peak not present in the H187Q UDG spectrum is the one in the box, which aligns exactly with the upfield peak (His187) in the 1D CBCA(CO)NH spectrum. (C) A 2D $^1H-^1H$ strip from the 3D ^{15}N-edited NOESY experiment ($^{15}N = 117.9$ ppm) shows an NOE correlation from the H^N of His187 to a proton with a chemical shift of 7.45 ppm, which exactly matches that of the H^{δ_2} of His187 shown in the 2D $^1H-^{15}N$ LR-HSQC spectra of free UDG (Figure 4). NOE correlations to other protons close in space to His187 H^N are also shown with potential assignments made as described in the text.

residues), except for the single peak enclosed in the box. This peak aligns exactly with the upfield H^N resonance in the 1D CBCA(CO)NH spectrum (Figure 5A) and is therefore assigned to His187. With this assignment in hand, we could search for NOE correlations between the H^N of His187 and its ring protons using the 3D ^{15}N-edited NOESY experiment.[3] A $^1H-^1H$ strip from the 3D ^{15}N NOESY spectrum (at the ^{15}N chemical shift of His187−N) shows a weak NOE correlation from the H^N of His187 to a proton with a chemical shift of 7.45 ppm (Figure 5C). This chemical shift exactly matches that of the H^{δ_2} proton of the spin system assigned to His187 in the $^1H-^{15}N$ LR-HSQC spectrum (Figure 4) and thus confirms our assignment of the His187 ring system.

The observation of this weak NOE correlation is in agreement with the crystal structure of free UDG, which shows a distance of 5.0 Å from His187 H^N to His187 H^{δ_2} (*7*). Also labeled in Figure 5C are the likely assignments for NOE correlations from His187 H^N to His187 H^α (2.9 Å) and H^{β_1,β_2} (2.3 and 2.5 Å), Gly165 H^N (3.5 Å) and H^{α_1,α_2} (2.9 and 3.7 Å), Pro186 H^α (2.5 Å) and H^{β_1,β_2} (2.9 and 3.4 Å), and Ser192 H^{β_1,β_2} (3.0 and 3.9 Å). These assignments are consistent with the random coil chemical shifts for protons in these residue types (*37*) and the distances between His187 H^N and these protons in the crystal structure of free UDG (*7*).

His187 Is Also Neutral in the Enzyme−Substrate Complex. The ionization state of His187 in the complex of UDG with the stable 2′-fluoro-2′-deoxyuridine substrate analogue, pU$^\beta$**P**A, was investigated using the LR-HSQC experiment (*9*, *18*). The analogue pU$^\beta$**P**A is an excellent substrate mimic because it is competitively displaced from UDG by uracil and the tighter binding substrate analogue AU$^\beta$A-5 (*9*). In addition, the K_D of 2.1 ± 0.1 μM for pU$^\beta$**P**A is similar to the K_m of 1.3 ± 0.2 μM for the corresponding 2′-β-H substrate pU**P**A (*9*). Finally, pU$^\beta$**P**A is hydrolyzed by UDG to uracil and abasic DNA but at a 10^7-fold slower rate than the corresponding 2′-β-H substrate pU**P**A ($t_{1/2}$ of pU$^\beta$**P**A ~70 days; data not shown). This 10^7-fold rate diminishment due to the 2′-β-F substitution is similar to that previously reported (*18*) and has no effect on the NMR experiments described below because the spectra were acquired in ≤2 days.

Figure 6 shows an overlay of the LR-HSQC spectra for the complexes of pU$^\beta$**P**A with wild-type UDG (black peaks) and H187Q UDG (red peaks). A comparison of the black and red peaks in Figure 6 shows that the spectra of the UDG−pU$^\beta$**P**A and H187Q−pU$^\beta$**P**A complexes overlay very well. The ^{15}N chemical shifts of all observable resonances are essentially identical in both spectra of Figure 6, with only minor perturbations in the ^1H chemical shifts of spin systems

[3] Attempts to make the connectivity from the backbone amide to the ring resonances of His187 using through-bond correlation experiments failed due to fast T_2 relaxation.

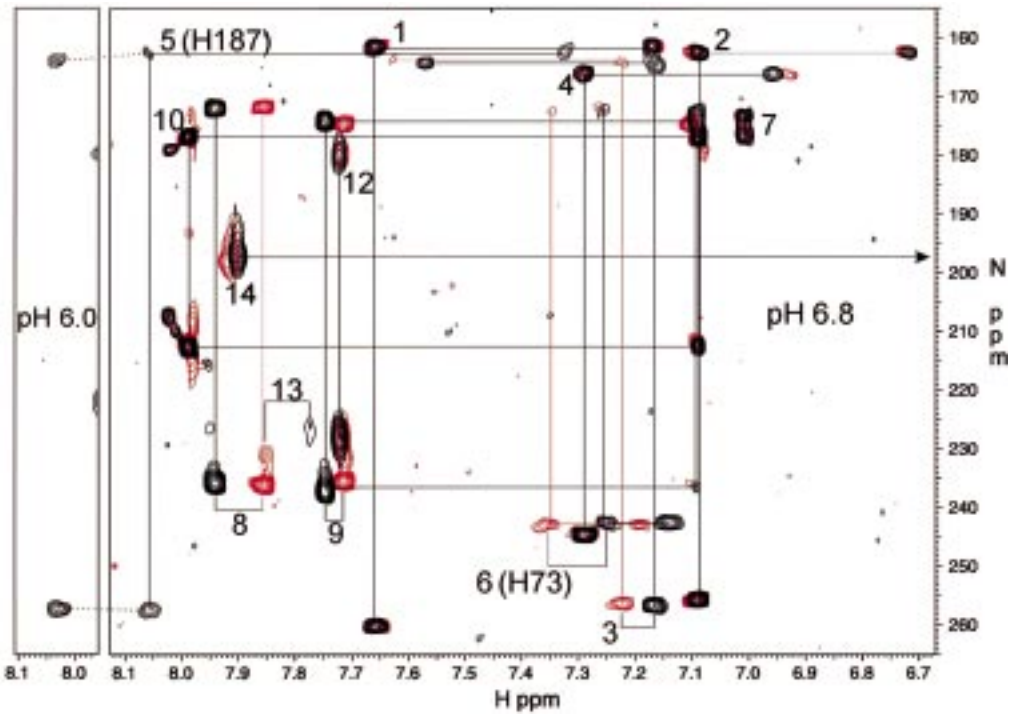

FIGURE 6: Overlay of the 2D $^1H-^{15}N$ LR-HSQC spectra for the complexes of pU$^{\beta}$**P**A with wild-type UDG (black peaks) and H187Q UDG (red peaks) at pH 6.8 and the His187 spectral region of the wild-type UDG−pU$^{\beta}$**P**A complex at pH 6.0. The spin systems are numbered to correspond with those in the free enzyme (Figure 4). A strip plot of the downfield resonances of His187 at pH 6.0 is also shown. Indicated by the arrow, the H^{δ_2} proton of system 13 resonates upfield at 5.97 ppm.

3, 6, 8, 9, and 13 ($\Delta\delta \leq 0.1$ ppm). Spin system 11 in the free UDG spectra (Figure 4) is absent in the spectra for both wild-type and H187Q UDG in complex with pU$^{\beta}$**P**A, presumably due to exchange broadening upon binding pU$^{\beta}$**P**A.

The assignment of the His187 spin system in the UDG−pU$^{\beta}$**P**A complex is based on two observations. First, the only spin system missing in the H187Q−pU$^{\beta}$**P**A spectrum that is present in the wild-type spectrum is that labeled 5 (His187) in Figure 6. Second, very little change in the $^1H-^{15}N$ chemical shifts of the His187 ring are seen when comparing the LR-HSQC spectra of free UDG and the UDG−pU$^{\beta}$**P**A complex (Figures 4 and 6, $\Delta\delta\ ^1H^{\delta_2} = 0.13$ ppm, $\Delta\delta\ ^1H^{\epsilon_2} = 0.02$ ppm, $\Delta\delta\ ^{15}N^{\delta_1} = 4.1$ ppm, and $\Delta\delta\ ^{15}N^{\epsilon_2} = 4.5$ ppm). From a comparison of the reference $^1H-^{15}N$ peak patterns in Figure 1 with those observed for the His187 pU$^{\beta}$**P**A spectrum (Figure 6), it is clear that *His187 remains neutral in the enzyme−substrate complex at pH 6.8*. To set limits on the pK_a for His187 in the enzyme−substrate complex, we collected the 2D LR-HSQC spectrum of the wild-type UDG−pU$^{\beta}$**P**A complex at pH 6.0 and found that His187 is also neutral at pH 6.0 (Figure 6). Thus, consistent with the pH dependence of k_{cat} (*9*), these NMR results require that the pK_a of His187 is ≤5.5 in the enzyme−substrate complex. These results effectively exclude the involvement of a cationic His187 in the catalytic mechanism of UDG.

Structural Basis for the Low pK_a of His187. Inspection of the crystal structures of free UDG, as well as the uracil and abasic DNA complexes, indicates that the less favorable ΔG for protonation of His187 relative to free imidazole, i.e., its low pK_a, is likely due to a significant and unfavorable reorganizational energy. This conclusion is based on the observation of a 2.9 Å hydrogen bond from the N^{δ_1} of His187 to the backbone nitrogen of Ser189 in the crystal structures of *E. coli* UDG and its uracil complex (Figure 3) (*7*). The same interaction is seen in the crystal structures of human UDG and its ternary complexes with uracil and duplex abasic DNA (*5*, *34*, *38*), and herpes virus UDG and its complex with uracil (*4*). Since this hydrogen bond must be broken before the His187 ring can become cationic, the apparent ΔG for protonation of His187 will include an unfavorable contribution from the work required for this reorganization.

Characterization of the 13 Other Histidines in UDG. Examination of the crystal structure and the 2D LR-HSQC NMR spectra of free *E. coli* UDG provides the specific assignment of one more histidine residue and narrows the possible assignments of four other histidine residues. Spin system 6 can be unambiguously assigned to His73, because only His73 has the hydrogen bonds required to stabilize the $N^{\delta_1}-H$ tautomeric form as observed for system 6 in Figures 4 and 6 (*7*). The assignment of spin systems 1 through 4 can be narrowed to His108, His136, His180, and His202, because only these histidine residues (with the exception of His187) have the hydrogen bonds required to stabilize the observed $N^{\epsilon_2}-H$ tautomeric form (Figure 4) (*7*). Spin systems 1 through 4 are also unique, because the nitrogen-attached H^{ϵ_2} proton was observed in 2D $^1H-^{15}N$ HSQC spectra optimized for one-bond $^1H-^{15}N$ correlations (not shown). This result indicates that exchange of the H^{ϵ_2} proton with solvent is inhibited. Accordingly, the crystal structure shows that each of these four histidines participates in an intramolecular hydrogen bond that could inhibit the exchange of H^{ϵ_2} with solvent (*7*). The remaining eight histidines are mostly solvent exposed, titrate in the pH range 6−7 (not shown), and remain unassigned. To our knowledge, this is the largest number of histidine ring systems resolved in a protein using NMR methods. The high resolution and sensitivity of the $^1H-^{15}N$ LR-HSQC experiment for histidine ring systems,

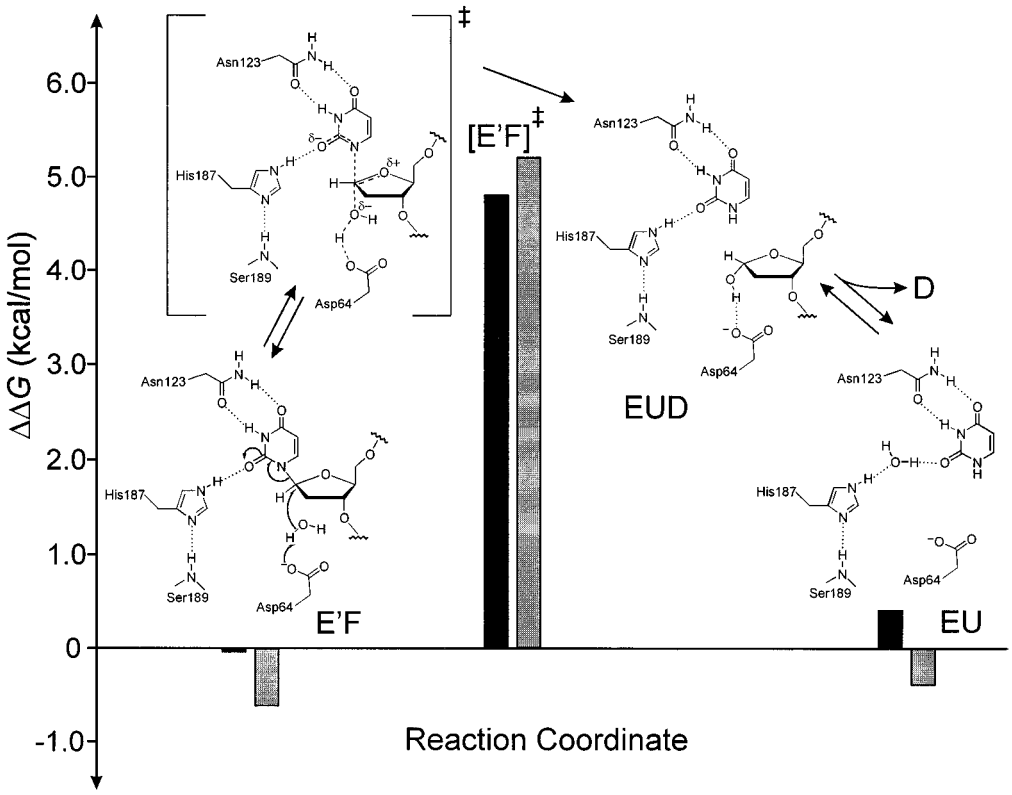

FIGURE 7: Catalytic mechanism for UDG and relative stabilities of complexes along the reaction pathway for H187Q (black) and D64N (gray) UDG. The relative stabilities are expressed as difference free energies ($\Delta\Delta G = \Delta G^{mut} - \Delta G^{wt}$). The free energies for the ground state complexes were calculated from the measured binding constants for AU$^{\beta}$A-5 and uracil (*9*) using the Gibbs equation $\Delta G° = -RT \ln(1/K_D)$, and the activation free energies were calculated from $\Delta G^{‡} = -RT \ln k_{max}(h/kT)$ using the k_{max} value of 150 s^{-1} for AU**P**-5 (*9*). The difference free energies are shown for the flipped-out uridine nucleotide complex (E′F), the transition state ([E′F]‡), and the uracil product complex (EU) following release of the abasic DNA product (D) (*9*). A distinct conformational form of the enzyme is designated by E′ on the basis of previous structural and kinetic studies (*18*, *34*). The side chain groups of Asp64 and His187 stabilize the transition state significantly but the ground states only weakly (*9*). The proposed mechanism involves concerted general base catalysis by Asp64 and electrophilic stabilization of the developing enolate on uracil O2 by a neutral His187. In accord with the crystal structure of the UDG−uracil complex (*7*), a water molecule is shown bridging His187 N^{ϵ_2}−H and uracil O2 in the EU complex. The contribution of Asn123 to transition state stabilization is not yet clear because substitution of valine for this group in the human enzyme resulted in large effects on both DNA binding and catalysis (*38*).

even for a complex system such as UDG, suggest it may be used effectively for other proteins of similar size and complexity.

A comparison of Figures 4 and 6 shows that the histidine ring systems seen in the UDG−pU$^{\beta}$**P**A complex spectra are in the same tautomeric state with similar ^{15}N chemical shifts as for free UDG. The two exceptions are system 11, which is absent in the spectrum for the complex, and system 12, which shows greatly diminished intensity. Both of these effects are probably due to exchange broadening upon forming the complex with pU$^{\beta}$**P**A. The exchange broadening of two histidine ring spin systems is not unexpected, since His67 and His134 are in the DNA binding cleft of UDG (*7*).

Weak Hydrogen Bonding to Uracil O2 in the Enzyme−Substrate Complex. The His187 N^{δ_1} and N^{ϵ_2} resonances show changes in ^{15}N chemical shift upon forming the complex with pU$^{\beta}$**P**A (Figures 4 and 6), which may reflect a weakening of the hydrogen bonds involving these atoms upon forming the enzyme−substrate complex. The upfield ^{15}N resonance of His187 (N^{ϵ_2}−H) moves *further upfield* by 4.5 ppm upon forming the pU$^{\beta}$**P**A complex, similar to the ∼4 ppm upfield change seen for the $^{15}N^{\delta_1}$ nitrogen of N^{δ_1}-methylimidazole in going from water, a good hydrogen bond acceptor, to benzene or chloroform, which are poor hydrogen bond acceptors (*16*). This result suggests that the hydrogen bond between His187 N^{ϵ_2}−H and uracil O2 in the enzyme−substrate complex is weaker than the 2.6 Å hydrogen bond between His187 N^{ϵ_2}−H and an ordered water molecule in free UDG (*7*) and is consistent with the small effect of the H187Q mutation on the stability of the enzyme−substrate complex (*9*). The downfield ^{15}N resonance of His187 (N^{δ_1}) moves *further downfield* by 4.1 ppm upon forming the pU$^{\beta}$**P**A complex. This may be compared with the 9 and 17 ppm downfield changes for the N^{ϵ_2} nitrogen of N^{δ_1}-methylimidazole in going from water to benzene and chloroform, respectively (*16*). This suggests that the hydrogen bond between His187 N^{δ_1} and Ser189 H^N in free UDG (*7*) may also be weakened upon formation of the enzyme−substrate complex.

Role for Neutral Electrophiles in Enzymatic Catalysis. The question of why a neutral electrophile has been selected by evolution to stabilize a negatively charged transition state has been encountered previously by Lodi and Knowles in their studies of triosephosphate isomerase (TIM). Similar to our findings, His95 of TIM has a pK_a below 4.5, which was partially attributed to a hydrogen bond from the backbone amide of Glu97 to the N^{δ_1} of His95. In addition, TIM stabilizes an enediolate transition state that is similar to the suggested O2 enolate transition state in the UDG reaction

(*12*). The observation that these two enzymes use neutral electrophiles is somewhat surprising, because simple electrostatic considerations suggest that a cationic electrophile should provide greater catalysis by preferential stabilization of a negatively charged transition state over that of a neutral ground state. The selection for a neutral electrophile may simply reflect that the nonpolar active site of UDG required for catalysis cannot accommodate a cationic electrophile. An additional advantage of a neutral histidine may be that its pK_a would approximate that of the enolic transition state (pK_a $\sim$ 10−13) (*39*, *40*). This matching of pK_a values between donor and acceptor would increase the hydrogen bond energy in the transition state, as discussed below (*12*, *41*). Finally, it has been proposed that matching pK_a values in the transition state can allow formation of a low-barrier hydrogen bond (LBHB) (*42*). Such a LBHB was proposed for TIM (*43*, *44*), but recent NMR studies suggest that a regular hydrogen bond is sufficient to account for the contribution of His95 to catalysis (*45*). Currently, we have no evidence that a LBHB is involved in the UDG reaction (*9*).

Can a Neutral Hydrogen Bond Account for the 4.8 kcal/mol Transition State Stabilization of His187? Shan and Herschlag have conducted model studies that directly address the energetics of hydrogen bond formation between a neutral donor and a negatively charged acceptor (*41*). In this work, the free energy of hydrogen bonding (ΔG^{HB}) was determined as a function of the pK_a difference between the donor and acceptor (ΔpK_a). A linear dependence of ΔG^{HB} upon ΔpK_a was observed, with a much steeper dependence in dimethyl sulfoxide ($\Delta G^{HB}/\Delta$pK_a = 1.0 kcal/mol) than in water ($\Delta G^{HB}/\Delta$pK_a = 0.07 kcal/mol) (*41*). The steeper dependence of ΔG^{HB} on ΔpK_a in DMSO is most simply explained by the greater Coulombic attraction between the partial effective charges on the donor and acceptor in this less polar solvent. These results suggest that a hydrogen bond between a donor−acceptor pair in a nonaqueous enzyme active site would be stronger than the corresponding hydrogen bond in water and would approach a maximum as ΔpK_a approached zero. In the case of UDG, the ΔpK_a between His187 N^{ϵ_2}−H and uracil O2 may decrease by at least 14 pK_a units, as uracil O2 converts from a carbonylic oxygen in the ground state (pK_a = −3.7) to an enolic oxygen in the transition state (pK_a $\sim$ 10−13). Accordingly, if the UDG active site resembles DMSO, the transition state could be stabilized by 14 kcal/mol relative to the ground state [$\Delta\Delta G^{HB} = \Delta$p$K_a(\Delta G^{HB}/\Delta$p$K_a)^{DMSO} = 14 \times 1.0 = 14$]. Alternatively, if the UDG active site resembles an aqueous environment, the selective stabilization would only be 1 kcal/mol [Δp$K_a(\Delta G^{HB}/\Delta$p$K_a)^{H_2O} = 14 \times 0.07 = 1$]. Although there is uncertainty in directly relating a mutagenic effect to hydrogen bond energy, these approximations show that a neutral hydrogen bond from His187 N^{ϵ_2}−H to uracil O2 in a moderately nonpolar active site could easily account for the experimentally observed 4.8 kcal/mol transition state stabilization attributed to His187 (*9*).

Conclusion. The catalytic mechanism of uracil glycosidic bond cleavage by uracil DNA glycosylase has been elucidated (Figure 7). We propose a concerted mechanism of electrophilic and general base catalysis by His187 and Asp64, respectively, on the basis that (i) these residues interact weakly with the ground state and strongly with the transition state and (ii) His187 is neutral such that preequilibrium protonation of uracil in the ground state is energetically untenable. In general, a concerted mechanism may be required for hydrolysis of the glycosidic bond in pyrimidine bases because of the highly unfavorable thermodynamics for protonating the pyrimidine carbonyl oxygens in the ground state. This concerted mechanism differs considerably from the mechanism suggested for several purine *N*-ribohydrolases, which involves *preequilibrium* protonation of the purine base in the enzyme−substrate complex (*46*, *47*). Thus, similar to the reactions in aqueous solution, the mechanism of enzyme-mediated glycosidic bond cleavage in pyrimidine and purine nucleosides is determined by the acidity of the leaving base.

ACKNOWLEDGMENT

The authors thank Andrew Howard of the Biological, Chemical, and Physical Sciences Department, Illinois Institute of Technology, for use of the Argonne Advanced Photon Source IMCA-CAT beamline for X-ray data collection and for his help in data processing.

REFERENCES

1. Zoltewicz, J. A., Clark, F. D., Sharpless, T. W., and Grahe, G. (1970) *J. Am. Chem. Soc. 92*, 1741−1750.
2. Garrett, E. R., and Mehta, P. J. (1972) *J. Am. Chem. Soc. 94*, 8542−8547.
3. Shapiro, R., and Danzig, M. (1972) *Biochemistry 11*, 23−29.
4. Savva, R., McAuley-Hecht, K., Brown, T., and Pearl, L. (1995) *Nature 373*, 487−493.
5. Slupphaug, G., Mol, C. D., Kavli, B., Arvai, A. S., Krokan, H. E., and Tainer, J. A. (1996) *Nature 384*, 87−92.
6. David, S. S., and Williams, S. D. (1998) *Chem. Rev. 98*, 1221−1261.
7. Xiao, G., Tordova, M., Jagadeesh, J., Drohat, A. C., Stivers, J. T., and Gilliland, G. L. (1999) *Proteins 35*, 13−24.
8. Shroyer, M. J. N., Bennett, S. E., Putnam, C. E., Tainer, J. A., and Mosbaugh, D. W. (1999) *Biochemistry 38*, 4834−4845.
9. Drohat, A. C., Jagadeesh, J., Ferguson, E., and Stivers, J. T. (1999) *Biochemistry 38*, 11866−11875.
10. Bachovchin, W. W., and Roberts, J. D. (1978) *J. Am. Chem. Soc. 100*, 8041−8047.
11. Bachovchin, W. W. (1986) *Biochemistry 25*, 7751−7759.
12. Lodi, P. J., and Knowles, J. R. (1991) *Biochemistry 30*, 6948−6956.
13. Pelton, J. G., Torchia, D. A., Meadow, N. D., and Roseman, S. (1993) *Protein Sci. 2*, 543−558.
14. Witanowski, M., Stefaniak, L., Januszewski, H., Grabowski, Z., and Webb, G. A. (1972) *Tetrahedron 28*, 637−653.
15. Blomberg, F., Maurer, W., and Ruterjans, H. (1977) *J. Am. Chem. Soc. 99*, 8149−8159.
16. Farr-Jones, S., Wong, W. Y. L., Gutheil, W. G., and Bachovchin, W. W. (1993) *J. Am. Chem. Soc. 115*, 6813−6819.
17. Van Dijk, A. A., Scheek, R. M., Dijkstra, K., Wolters, G. K., and Robillard, G. T. (1992) *Biochemistry 31*, 9063−9072.
18. Stivers, J. T., Pankiewicz, K. W., and Watanabe, K. A. (1999) *Biochemistry 38*, 952−963.
19. Neidhardt, F. C., Bloch, P. L., and Smith, D. F. (1974) *J. Bacteriol. 119*, 736−747.
20. Howard, A. J., Gilliland, G. L., Finzel, B. C., Poulos, T. L., Ohlendorf, D. H., and Salemme, F. R. (1987) *J. Appl. Crystallogr. 20*, 383−387.
21. Sheldrick, G. M. (1997) *SHELX-97*, University of Gottingen, Gottingen, Germany.
22. Sheldrick, G. M., and Schneider, T. R. (1997) *Methods Enzymol. 277*, 319−343.
23. Roussel, A., Inisan, A. G., and Cambillau, C. (1996) *TURBO-FRODO*, AFMB and Bio Graphics, Marseille, France.
24. Laskowski, R. A., McArthur, M. W., Moss, D. S., and Thornton, J. M. (1993) *J. Appl. Crystallogr. 26*, 283−291.

25. Wishart, D. S., Bigam, C. G., Yao, J., Abildgaard, F., Dyson, H. J., Oldfield, E., Markley, J. L., and Sykes, B. D. (1995) *J. Biomol. NMR 6*, 135−140.
26. Marion, D., Ikura, M., Tschudin, R., and Bax, A. (1989) *J. Magn. Reson. 85*, 393−399.
27. Delaglio, F., Grzesiek, S., Vuister, G. W., Zhu, G., Pfeifer, J., and Bax, A. (1995) *J. Biomol. NMR 6*, 277−293.
28. Mori, S., Abeygunawardana, C., Johnson, M. O., and van Zijl, P. C. (1995) *J. Magn. Reson. B 108*, 94−98.
29. Shaka, A. J., Keeler, J., and Freeman, R. (1983) *J. Magn. Reson. 53*, 313−340.
30. Shaka, A. J., Barker, P., and Freeman, R. (1985) *J. Magn. Reson. 64*, 547−552.
31. Kay, L. E., Marion, D., and Bax, A. (1989) *J. Magn. Reson. 84*, 72−84.
32. Grzesiek, S., and Bax, A. (1992) *J. Am. Chem. Soc. 114*, 6291−6293.
33. Ramachandran, G. N., Ramakrishnan, C., and Sasisekharan, V. J. (1963) *J. Mol. Biol. 7*, 95−99.
34. Parikh, S. S., Mol, C. D., Slupphaug, G., Bharati, S., Krokan, H. E., and Tainer, J. A. (1998) *EMBO J. 17*, 5214−5226.
35. Bycroft, M., and Fersht, A. R. (1988) *Biochemistry 27*, 7390−7394.
36. Shortle, D. (1994) *J. Magn. Reson. B 105*, 88−90.
37. Wuthrich, K. (1986) in *NMR of Proteins and Nucleic Acids*, John Wiley & Sons, Inc., New York.
38. Mol, C. D., Arvai, A. S., Slupphaug, G., Kavli, B., Alseth, I., Krokan, H. E., and Tainer, J. A. (1995) *Cell 80*, 869−878.
39. Kresge, A. J. (1991) *Pure Appl. Chem. 63*, 213−221.
40. Stivers, J. T., Abeygunawardana, C., Mildvan, A. S., Hajipour, G., and Whitman, C. P. (1996) *Biochemistry 35*, 814−823.
41. Shan, S. O., and Herschlag, D. (1996) *Proc. Natl. Acad. Sci. U.S.A. 93*, 14474−14479.
42. Cleland, W. W., Frey, P. A., and Gerlt, J. A. (1998) *J. Biol. Chem. 273*, 25529−25532.
43. Gerlt, J. A., and Gassman, P. G. (1993) *Biochemistry 32*, 11943−11952.
44. Cleland, W. W., and Kreevoy, M. M. (1994) *Science 264*, 1887−1890.
45. Harris, T. K., Abeygunawardana, C., and Mildvan, A. S. (1997) *Biochemistry 36*, 14661−14675.
46. Mentch, F., Parkin, D. W., and Schramm, V. L. (1987) *Biochemistry 26*, 921−930.
47. Horenstein, B. A., Parkin, D. W., Estupinan, B., and Schramm, V. L. (1991) *Biochemistry 30*, 10788−10795.

BI9910880